Europa Kinetic Ice Penetrator System for Hyper Velocity Instrument Deposition

Tessa Robinson

A thesis

submitted in partial fulfillment of the

requirements for the degree of

Master of Science in Aeronautics & Astronautics

University of Washington

2016

Committee:

Robert Winglee

Carl Knowlen

University of Washington

Abstract

Europa Kinetic Ice Penetrator System for Hyper Velocity Instrument Deposition

Tessa Robinson

Chair of the Supervisory Committee:

Dr. Robert Winglee

Earth and Space Science / Aeronautics and Astronautics

Landing of a payload on any celestial body has only used a soft landing system. These systems use retro rockets and atmospheric components to match velocity and then overcome local gravity in order to land on the surface. This is a proposed system for depositing instrumentation on an icy surface at hypervelocity using the properties of different projectiles and ejecta properties that would negate the need for a soft landing system. This system uses two projectiles, a cylinder with inner aerodynamic surfaces and a payload section with a conical nose and aerodynamic surfaces. The cylinder lands first, creates a region of fractured ice, and directs that fractured material into a collimated ejecta stream. The payload travels through the ejecta and lands in the fractured region. The combination of the ejecta stream and the softened target material reduces the impact acceleration to within survivable levels.

Dedication

Deborah Hughes for showing me how awesome space and space travel are

Mendi Norris and Gloria Sheppard for leading me to this degree path and for knowing I could do this before I did.

Robert Dougherty for giving me the opportunity to be great at what I do.

Judith and Charles Robinson for teaching me humility rooted in love and confidence rooted in sober reflection.

Contents

History

Asteroid Penetrator

The University of Washington Advanced Propulsion Lab developed a concept for asteroid sample extraction. The system has a penetrator body with a sample return container, SRC, inside of it. As the system approaches an asteroid or comet, it doesn't do a standard delta-V maneuver to match the asteroid speed for rendezvous. Instead it uses the difference in velocity to impact the asteroid. As the outer body penetrates the asteroid, sample material fills up the SRC. As the SRC is filled, it ejects out the back of the main body. A tether on the SRC connected to either a skycrane type orbiter or the initial satellite/probe is retracted for collection. The main orbiter can then return to the Earth-Moon system for analysis. [1]

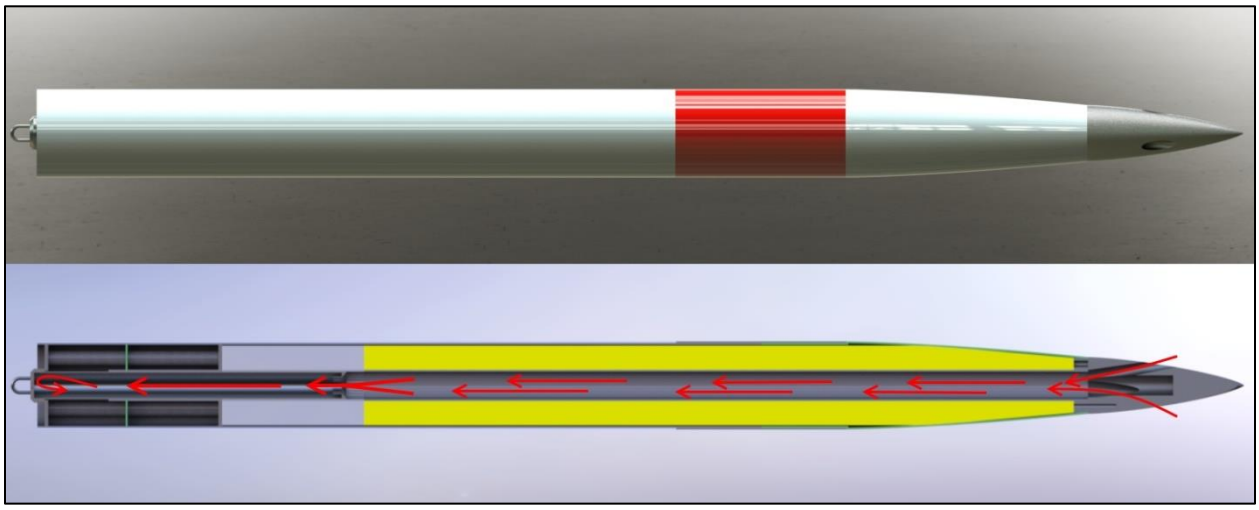

Figure 1: Early Iteration of Asteroid Penetrator System [1]

Several iterations of the nose cone/SRC system were tested. The nose cone with multiple side ports for collection had a stagnation effect that prevented the SRC from filling completely. The nose cone with a center bore and side ports allowed for filling of the SRC but

the sample had possible morphic effects due to turbulent boundary effects which could affect the post-analysis process.

Figure 2: Center Bore and Side Port SRC Sample with Concentric Ring Possibly Caused by Boundary Effects [1]

The most successful system had only a center bore with the SRC lined up either just ahead of the end of the nose cone or even with the front edge. The outer diameter of the SRC is less than the inner diameter of the ejection chamber which allows for ejection even in the case of chamber buckling.

Figure 3: Close Up of Close Fitting Ejection Chamber Buckling with Impinged SRC [1]

Figure 4: Successfully Ejected SRC from System with Oversized Ejection Chamber [1]

Ice Cratering vs. Temperature

The study of the characteristics of ice impacts at a wide range of temperatures, 100K to 235K, shows that the hardness of the ice increases as the temperature decreases. [2] The shape of the projectiles in this study was spherical, 1mm diameter and 1.43 mg mass, with an impact speed of $\sim 5 \frac{km}{s}$ into ice of varying temperatures. The shape of the cratering is consistent with meteoric impacts on rocky bodies such as Earth or Luna. The area of damage is

wide and the walls are shallow. The ejecta spray is wide and is not collimated. Due to increased hardness, the penetration decreases as temperature decreases. [2]

Table 1: Penetration Depths For 1mm Alum Projectiles Into Ice at Varying Temperatures [2]

Temperature (K)	Velocity $\left(\frac{km}{s}\right)$	Crater Diameter (mm)	Pit Diameter (mm)	Pit Depth (mm)
253	5.26	45.4	15.00	9.51
237	5.02	49.0	12.00	8.95
228	5.09	38.5	11.00	8.94
190	5.17	45.6	7.00	8.24
164	4.92	49.0	8.00	7.13
152	5.02	44.5	11.00	6.18

Empirical Penetration Depth Formula

An empirical formula was developed to predict penetration depth of various missile types in various target materials. [3] The various variables are changed based on the shape of the nose cone, projectile mass, projectile length, and impact velocity. The target material is accounted for with an empirical target coefficient to allow for varying hardness. [3]

$$D = \alpha K_s S N \left(\frac{m}{A}\right)^{0.7} (V_s - 30.5) \quad (1)$$

Where

$D = depth\ of\ penetration\ in\ meters$

$\alpha = 0.0000175 = 1.75 \times 10^{-5}$

$K_s = scaling\ factor$

$S = empirical\ target\ coefficient$

$N = penetrator\ nose\ coefficient$

$m = penetrator\ mass\ in\ kg$

$A = penetrator\ cross\ sectional\ area\ in\ m^2$

$V_s = impact\ velocity\ \frac{m}{s}$

For velocity regimes $\gg 30\frac{m}{s}$, equation (1) reduces to the following.

$$D = \alpha K_s S N \left(\frac{m}{A}\right)^{0.7} V_s \tag{2}$$

The scaling factor for hard targets is 1 for projectile mass greater than 182kg. For smaller projectiles, the scaling factor is mass dependent.

$$for\ mass < 182\text{kg}\ \ K_s = 0.46 \times m^{0.15} \tag{3}$$

The penetrator nose cone coefficient for a conical shape is defined as below.

$$N = 0.26\left(\frac{L_n}{d}\right) + 0.56 \tag{4}$$

Where

$L_n - length\ of\ penetrator\ nose\ in\ m$

$d - diameter\ of\ penetrator\ in\ m$

For a flat nose cone, this yields $N = 0.56$. For a sharp cone of $\frac{L_n}{d} = 4$, this yields $N = 1.6$. This demonstrates that the shape of the nose cone can alter penetration depth 2 to 3 times, but will not change by an entire order of magnitude.

The factor mass/area in equation (2), can be expressed as density over penetrator length, ρL . This relationship demonstrates how the overall shape of a penetrator affects penetration

depth. A short and wide projectile will have a significantly shorter stopping distance than a long and thin projectile. As final designs of a projectile are made, the balance between longer penetration depth and structural integrity must be balanced.

The empirical target coefficient varies depending on the target material:

Medium Strength Rock	$S \sim 0.8$	ex: Basalt
Low Strength Rock	$S \sim 1.3$	ex: Sandstone
Silty Clay	$S \sim 8$	

Engineering Problem

Jupiter's moon Europa has an icy crust with an underground ocean of liquid water. This large ocean is one of the best locations for life to have possibly developed and is therefore a prime objective for scientific study.

The first step is orbital studies to measure overall characteristics such as magnetic field, gravitational field, and imagery on visible and non-visible spectrums. The second step is to get onto the surface for more in-depth study. These measurements can include magnetic studies, salinity and other chemical measurements, and seismic activity which could determine if the surface behaves similarly to tectonic plates on Earth. The third step is to get below the icy surface to the liquid underneath. This can be done through drilling or melting using resistive or RTG heating. This research is focused on a method for instrument deposition on the surface of Europa.

The standard method for depositing payloads is a soft landing. This requires rockets and the associated fuel, fuel systems, and control systems. Europa doesn't have an atmosphere thick enough for aerobraking tools such as an aeroshell or parachutes.

A hard landing would be a lower mass option of payload deposition. The maximum acceleration of such a landing needs to be less than 100-200 km/s^2. This is the highest level of acceleration that military grade electronics can survive Projectile shape, penetration depth, and ejecta plume characteristics can be determined and combined to keep maximum acceleration within acceptable levels.

Potential System Proposals

The two main types of hard landing systems are a single projectile system and a multi-projectile system. The analysis of each system must determine if the maximum acceleration can be kept below survivable levels. The method for determining this initially is a penetration depth calculation. The secondary level of analysis must determine if the target material properties can be altered to allow for sufficient penetration depth or if there are other impact characteristics and behavior which can allow for a longer stopping distance.

The minimum required stopping distance, assuming a constant acceleration, can be calculated from a basic kinematic equation, eqn. (5). For maximum acceleration, $a = 100\,\frac{km}{s^2}$, and initial velocity, $v_o = 4\,\frac{km}{s}$, this equation yields a minimum stopping distance, $d \cong 80m$.

$$v_f = v_o + 2a\Delta x \;\Rightarrow \Delta x = \frac{v_o^2}{2a} \tag{5}$$

The target material coefficient for ice can be calculated using the penetration depth data from Grey, et al. and the empirical penetration depth formula. This gives $S = 1.5$ for 100K ice and $S = 3$ for 253K ice. Assuming a 5kg projectile with a diameter of 10cm and using the 100K target coefficient, the predicted penetration depth is 0.25m which is at least 2 orders of magnitude too short.

This prohibitively short stopping distance rules out a single projectile system for instrument deposition. A multi-projectile system must be determined. Having two projectiles land in the same location with a relatively long delay only takes into account material softening. The penetration depth can be recalculated using the empirical target coefficient for 253K ice. This only increases the possible penetration depth by a factor of two and is not sufficient for the 2-3 order of magnitude increase required. Some other material phenomena at the time of impact must be utilized for increasing the stopping distance of the second projectile.

During hypervelocity collisions, two major physical phenomena take place in the target material. The first phenomenon is cratering which represents the pressure wave from the collision traveling through material which causes fracturing and possibly phase changes. The second phenomenon is material ejection from inside the crater. The ejecta, if directed back toward the second projectile, could provide a high velocity field through which the second projectile passes. Drag force could increase the stopping distance to within necessary levels.

The two major initial impactor shapes we will consider are conical and cylindrical. The conical shape has well studied cratering characteristics. The cratering is wide with shallow walls, and the ejecta pattern is wide spread and non-collimated. This does not lead to a good field for the secondary projectile to travel through.

A cylindrical projectile does not have well studied cratering characteristics. Upon observation of the shape of a cylinder with a center bore, the target material fractured on impact has a direct path back toward the second projectile to create a collimated field, similar to the asteroid penetrator nose cone and SRC system studied by Winglee, et al. [1]

Numerical Simulation – ANSYS

Preliminary ANSYS simulations were run to gain intuition into what takes place during a hypervelocity impact in the first few moments. The material for all projectiles is steel. The target materials is concrete chosen as an analog for the hardness level of ice at super-cooled temperatures.

The first simulation is a two projectile system. Both projectiles are a simple conical shape nose cone with a solid cylindrical body.

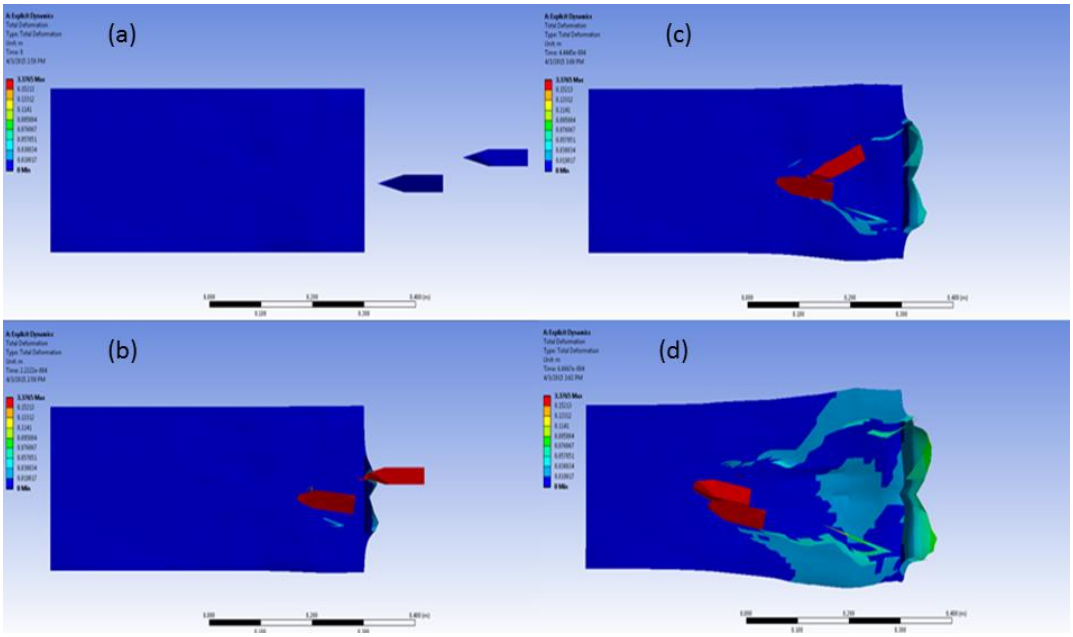

Figure 5 : ANSYS Simulation of Two Projectiles at 1 km/s

The projectiles were offset azimuthally by one diameter and offset in the direction of travel by one body length. The impact speed was 1 km/s. The first projectile deformed the material ahead of the second projectile. The second projectile traveled through the deformed or deforming material and was able to overtake the first projectile. This result provides proof of concept for the effect of target softening.

The second simulations were a single conical projectile and a single cylindrical projectile with a center bore. These simulations were run to show a comparison of target material deformation based on projectile shape.

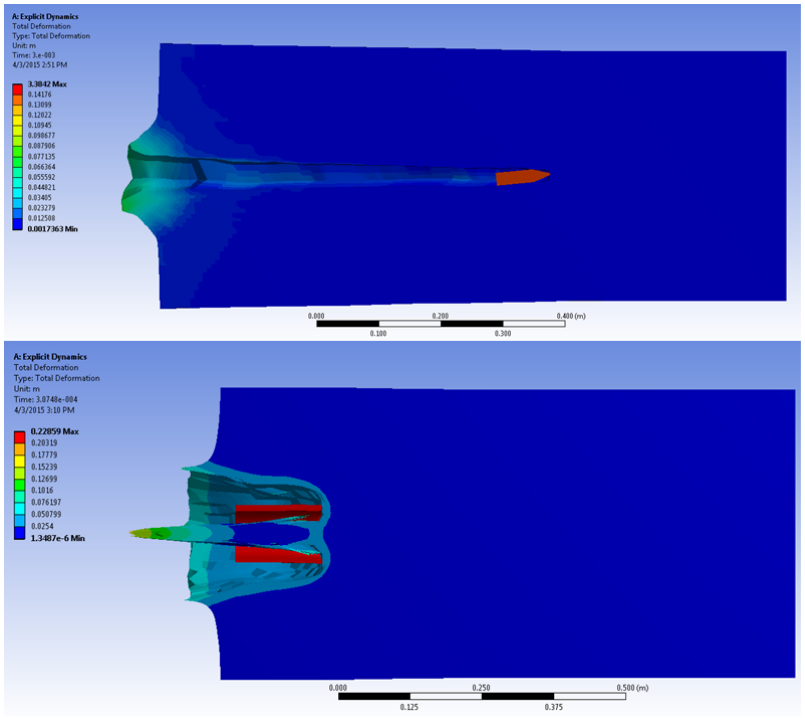

Figure 6: Comparison of Conical and Cylindrical Projectile Target Deformation

The cylindrical projectile creates an outward deformation with no collimated debris. The cylindrical projectile creates a more concentrated deformation region with a clearly collimated debris field.

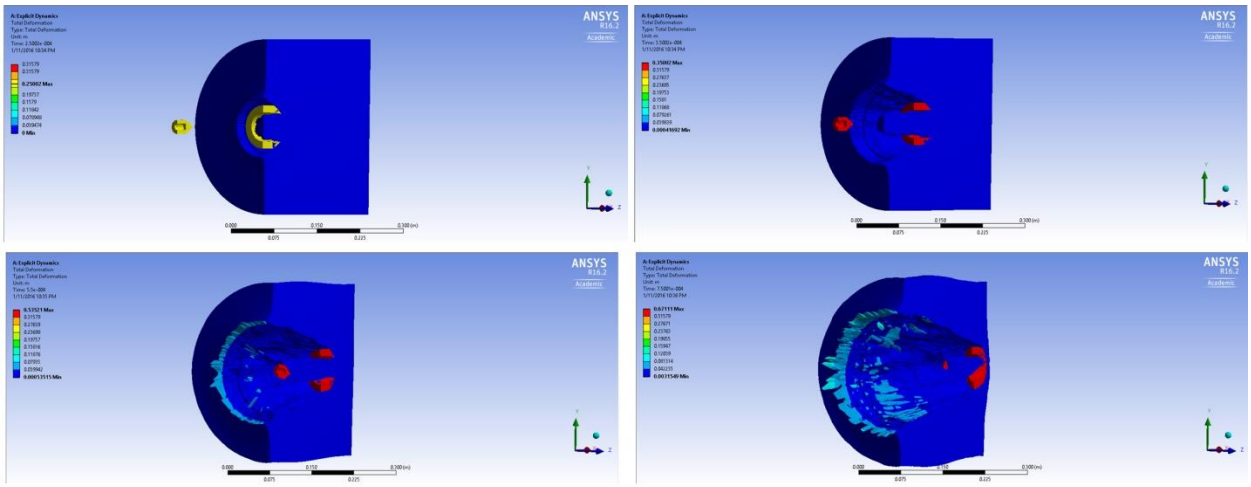

Figure 7: Two Projectile System with Cylindrical and Conical Systems

The third simulation was a two projectile impact of a cylindrical initial impactor followed by a conical projectile. An acceleration probe was placed on the second projectile for comparison to the acceleration profile of the single conical impact.

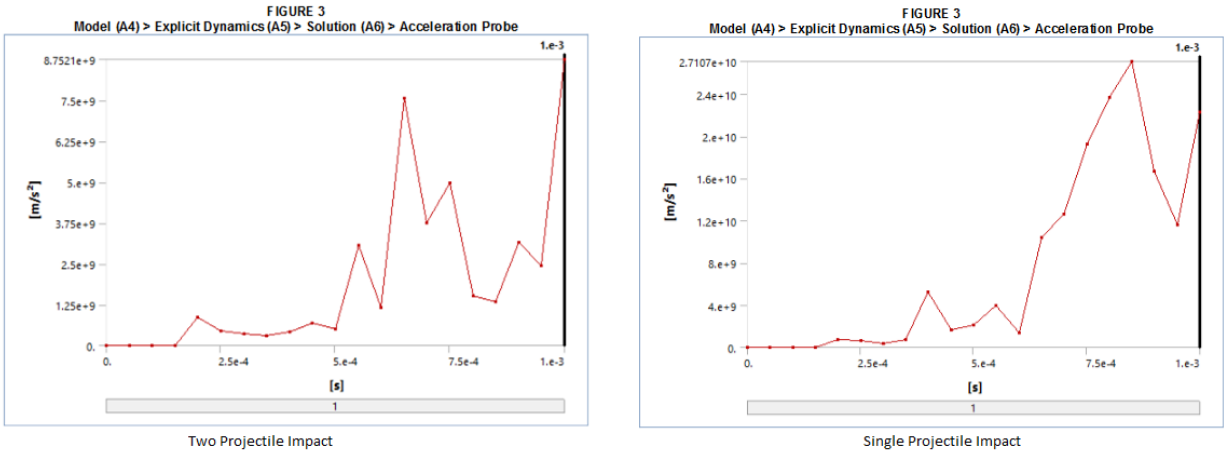

Figure 8: Comparison of Acceleration Probe Data for Single and Two Projectile Systems

The maximum acceleration for the two projectile system was reduced by an order of magnitude. The acceleration is still greater than the required maximum acceleration requirements; therefore target softening must be combined with the ejecta behavior for the final system.

Plume Estimation (First Order)

A calculation of the force required for negative acceleration of the second projectile within acceptable levels allows for a first order estimation of the necessary plume density. The density first calculated represents the density at the outermost edge of the plume and assumes that the change in density as the projectile through to the surface will produce a consistent acceleration profile.

$$F = ma \tag{6}$$

The assumed mass of the projectile is 5 kg. The projectile radius is assumed to be 5cm. The allowable acceleration is 100 km/s^2. Newton's second law, eqn. (6), shows a resulting force of $5 \times 10^5 N$.

$$F_{drag} = \frac{1}{2}\rho_o V^2 C_D A$$
$$\rho_o = \frac{2F}{V^2 C_D A} \tag{7}$$

Where

$V = 4000\,\frac{m}{s}$

$C_D = 0.5$

$A = \pi r^2 \quad with \;\; r = 5cm$

Substituting the force from eqn. (6) into the drag equation, eqn. (7), the required density is $16\,\frac{kg}{m^3}$. The inverse square law can be used as a basic assumption for density distribution of the plume. The plume height used is the minimum stopping distance of $H = 80m$.

$$\rho = \rho_o \left(\frac{H}{r}\right)^2 \tag{8}$$

Using a projectile radius as the height for the impact site, eqn. (8) shows a required density of $4 \times 10^7 \frac{kg}{m^3}$. The density of ice is $\sim 10^3 \frac{kg}{m^3}$, which is less than the required density at the impact site. Because of this discrepancy between the required density and the available density of material, the thin and conical shaped projectile design needs to be augmented.

When initially designing the kinetic impactor system, atmospheric effects were disregarded due to the lack of substantial atmosphere on the Europan surface. No aero surfaces were initially considered for either the first or second projectile. The plume generated by the first projectile can be thought of as a temporary atmosphere.

Of the factors in eqn. (7), the cross sectional area is the most easily altered. Adding aerodynamic surface area, such as an inflatable aero-shell, will increase the effective radius of the projectile and greatly affect the required density at the impact. Figure 9 shows a simple relationship between the effective radius and the resulting required density. Running this code out to a radius of 1m shows that increasing the radius under these current assumptions will lower the required density to less than the density of ice.

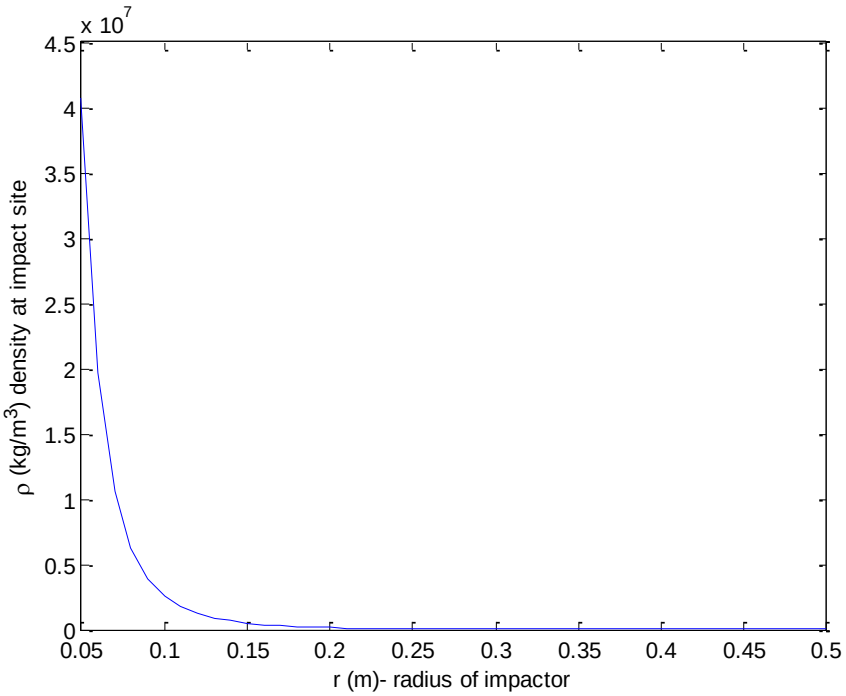

Figure 9: Required Density at Impact Site as a Function of Second Impactor Radius

The velocity and the density variation of the plume are two factors currently not well known. Empirical data on the shape and speed of the plume are necessary for a better understanding of what types of aero surfaces are needed for the second projectile.

Experimental Set-Up

The experimental goal for the first part of this research was to observe high velocity impact behavior of varying shapes with ice as the target material. A low pressure compressed air gun and a high pressure gas gun were used for testing. The air gun, though it generates low speeds, was used for rapid prototyping due to easier target set-up and short turn-over time between shots. The gas gun was used for higher velocity impacts.

Ice Targets

The initial ice targets were 30 gallon plastic trash cans filled with water and then frozen. The bins are sufficient size for air gun shots. They weigh $\sim 300\ lbs.$ and thus are transportable with a simple cart and 2-3 people. When used as targets for the helium gas gun, the energy involved in the impacts caused extensive damage to the cans.

Figure 10: 30 Gallon Ice Target and Cradle

The next size of can used was 96 gallons. High velocity shots, $> 1 \frac{km}{s}$, still caused damage to the larger cans, but the damage was greatly reduced. The next iteration for the 96 gallon cans will be an inner layer of insulation around a cylinder of water ice. The 96 gallon cans are $\sim 900\ lbs.$ and thus are more difficult to transport, but they can still be moved onto a flat cart by 4-5 people.

Figure 11: 96 Gallon Ice Target Lined With Pykrete

The insulation used inside the cans is Pykrete. Pykrete is a combination of woody fibrous material and water that is then frozen. The result is a higher strength material at approximately the same density as ice. [4]

After the Pykrete lined 96 gallon cans, 150 gallon water storage containers will be used. These larger containers will also be Pykrete lined, but the straighter sides of the container will allow for a significantly larger cylinder of water ice. These targets will weigh $\sim 1500\ lbs.$ and thus will need to have a cart permanently attached to allow for transport.

Freezing Process

The ice targets were made in a large industrial freezer with temperatures ranging from 253K to 238K. The targets were frozen in layers to prevent warping and rupture of the containers. They layering also allowed for a flat surface which is better for impact imaging.

For the larger containers, food coloring was added to each different layer. This coloring gives a visual representation of penetration depth for the impacts.

Low Pressure Compressed Air Gun

The air gun operates from 100 to 200 psi. The barrel is $\sim 2m$ long with a 5.715 cm (2.25”) inner diameter. The mass of the projectiles is $\sim 100\ gm$. The speed of the projectiles is around 120 m/s.

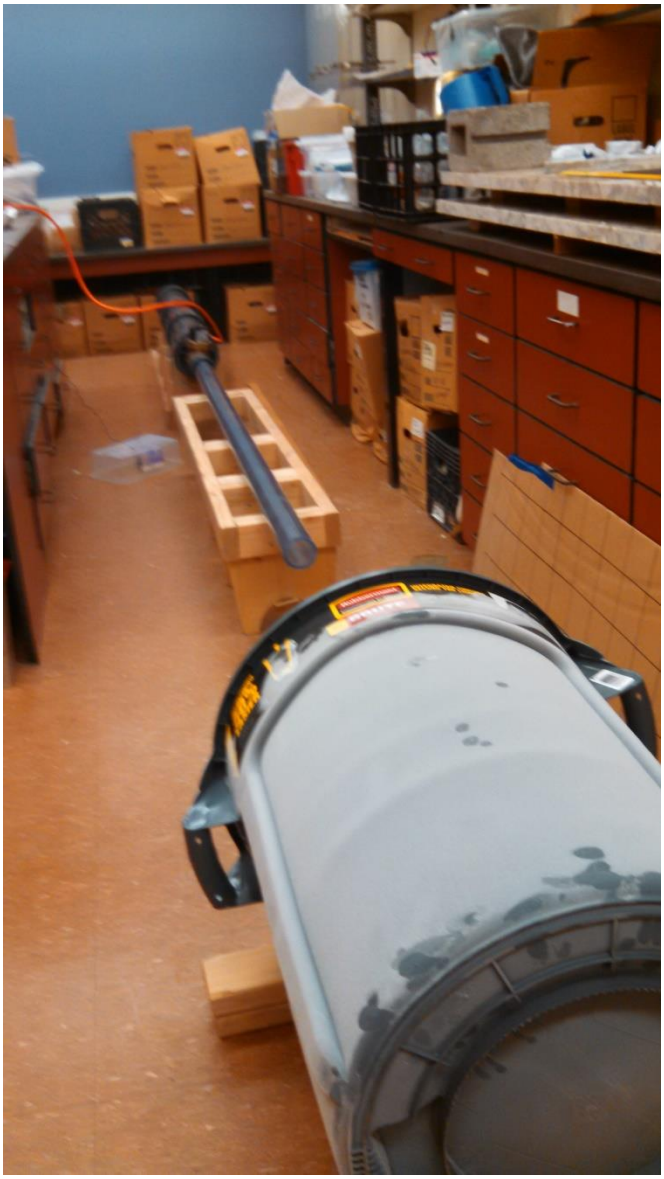

Figure 12: Low Pressure Air Gun Set-Up

The initial projectiles used were fiberglass cylinders filled with Kevlar encased electronic components. These shots tested if simple components could survive lower energy impacts, before trying to include them in high velocity impacts. Imaging for this gun has been 240 fps using a sport camera.

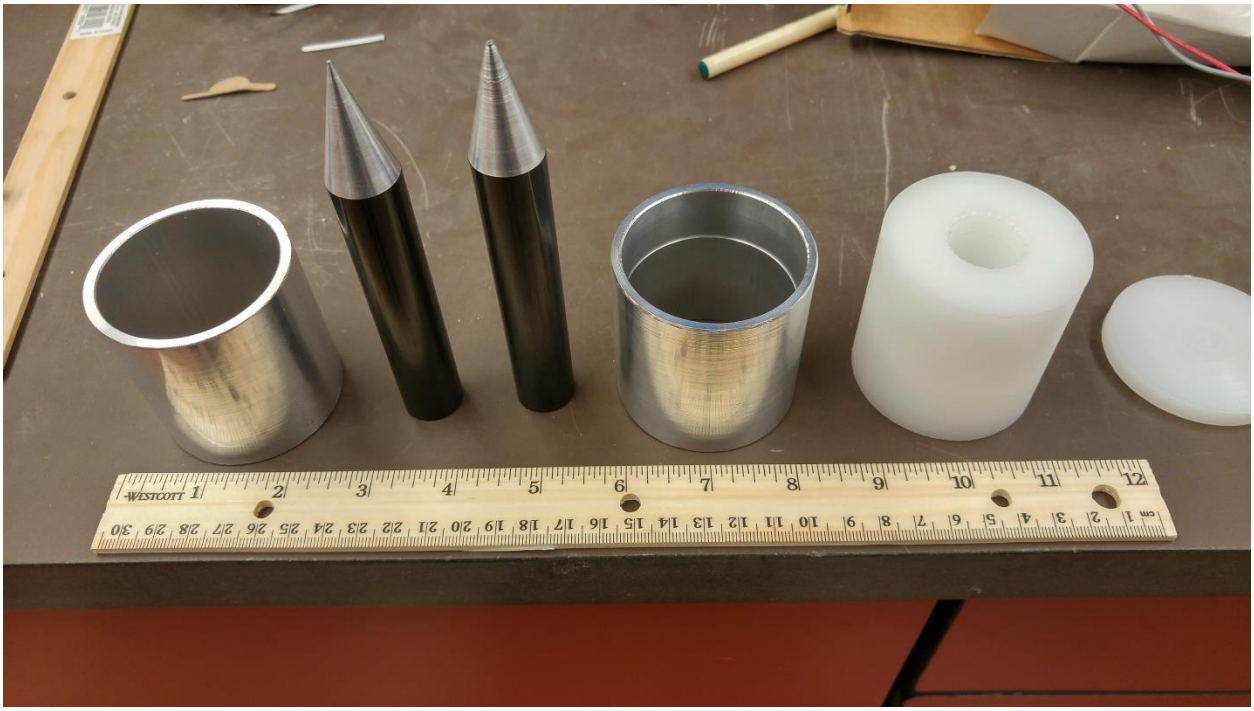

Figure 13: Low Pressure Air Gun Projectiles and Obturators

Figure 13 shows a collection of variousl projectiles. The main types of single projectiles were hollow cylinders and solid, and thin cylinders with conical nose cones. Each projectile was also shot with an obturator to provide a solid surface for the compressed air to push against. The projectiles are aluminum and the obturators are nylon.

Two projectile systems are currently being designed. A hollow cylinder is followed by a conical projectile. The conical projectile will contain an accelerometer circuit. Measurements will be taken of a conical projectile alone and then coupled with the hollow pre-impactor for comparison.

Figure 14: Two Projectile System for Accelerometer Deposition

High Pressure Gas Gun

Figure 15: RAM Lab Barrel

The helium gas gun is in the University of Washington RAM Accelerator and is extended in length by 15 m when using the test section in gun mode. The pressure for these experiments was in the range of 2000 to 5000 psi. The launch, $\sim 20m$ long, is pumped down to vacuum. Projectiles are $\sim 60\ g$ and reach speeds from 500 to 2000 m/s. Imaging for this gun has been 240 fps using sport cameras and 200,000 fps using a high speed camera.

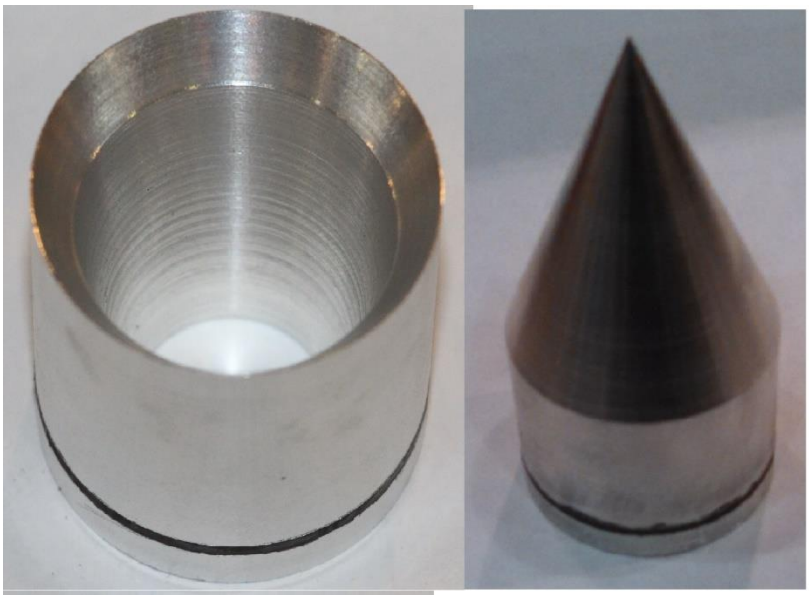

Figure 16: Cylindrical and Conical Projectiles for High Pressure Gas Gun

Figure 16 shows the two major types of projectiles and obturator used for this research. The diameter of the projectiles is 3.785 cm (1.49”). The projectiles for initial testing were Lexan and were shot into wood rounds. The projectiles for ice targets are aluminum and have had either aluminum or Lexan obturators.

Future projectiles will be a combination of steel, aluminum, and Lexan. The combined material projectiles will be a closer analog to the proposed system for Europa. The second projectile may contain an electronic component to test survivability.

Results

Low Pressure Air Gun

Fiberglass/Kevlar Projectiles

The first projectiles used for the low pressure gun system were fiberglass cylinders filled with Kevlar encased electronic components. Figure 17 has two projectiles of the same mass and composition. The projectile on the right was shot into the ice first. The Kevlar was displaced and the tape across the impact face was damaged during impact. The projectile on the left was shot into the same target at the same pressure. The Kevlar was displaced but not as far and the tape across the face showed significantly less damage. This was the first empirical demonstration of the concept of target softening.

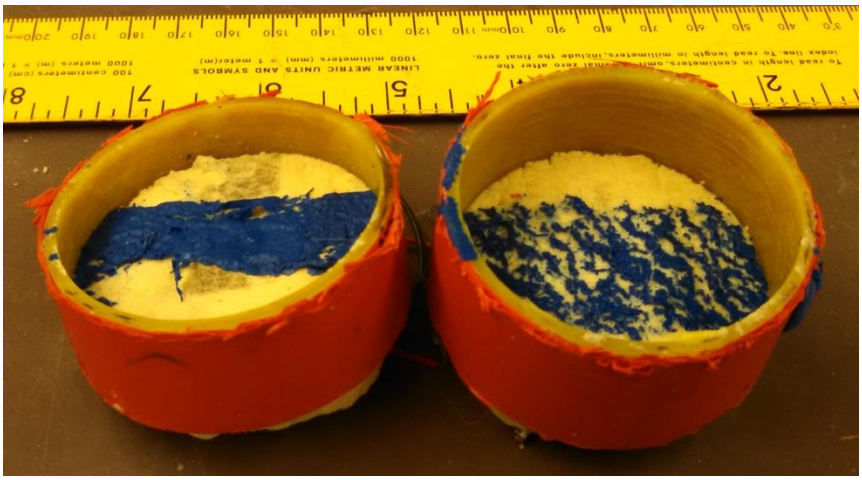

Figure 17: Kevlar and Fiberglass Projectiles Showing Differing Impact Energy from Tape Damage

Cratering Patterns

The difference in cratering patterns is demonstrated in figure 18. The conical projectile cratering is consistent with well-known cratering patterns. The width of the crater is wide and

the walls of the crater are shallow. The hollow cylindrical projectile crater is narrower and the walls are quite steep.

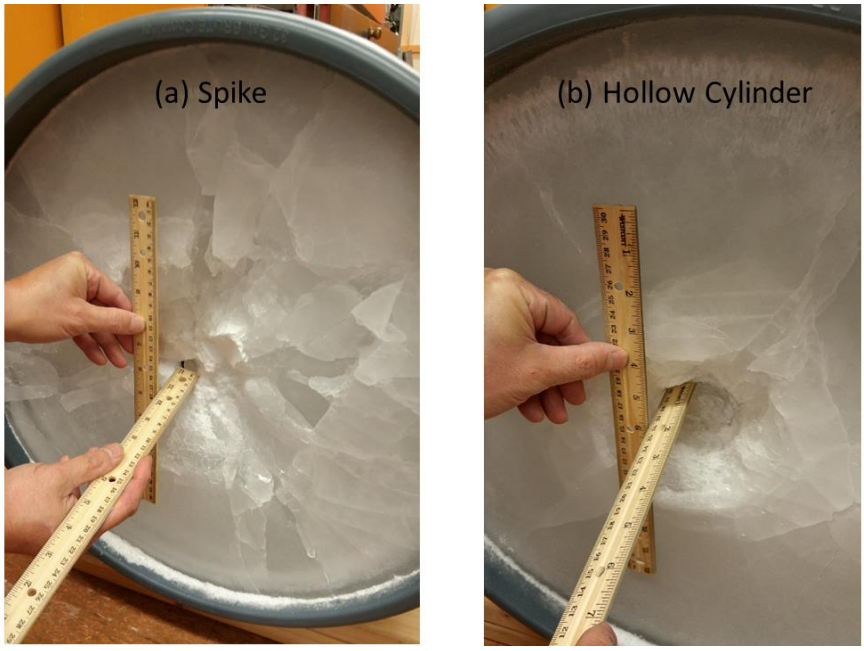

Figure 18: Low Pressure Air Gun Cratering Pattern Comparison

The shape for each type of cratering is significantly different, and the type of damage and debris are also significantly varied. The conical debris in figure 19 is mostly large fragments with very little powdering. This implies the impact energy was directed outward over a large area compared to the projectile size.

Figure 19: Conical Projectile Ejecta Debris

The cylindrical debris in figure 20 is highly powdered. The debris in this image was compressed into a cylinder by the obturator traveling behind the projectile and forming it into its cylindrical shape similar to shaping a snowball. This debris implies a highly concentrated region of damage to the target material.

Figure 20: Cylindrical Projectile Ejecta Debris

Ejecta

The ejecta stream produced during the hollow cylindrical projectile impact was highly concentrated. Frame (b) of figure 21 shows the column of ejecta traveling back through the cylinder. The ejecta spray produced during the conical projectile impact was wide spread and contained large pieces.

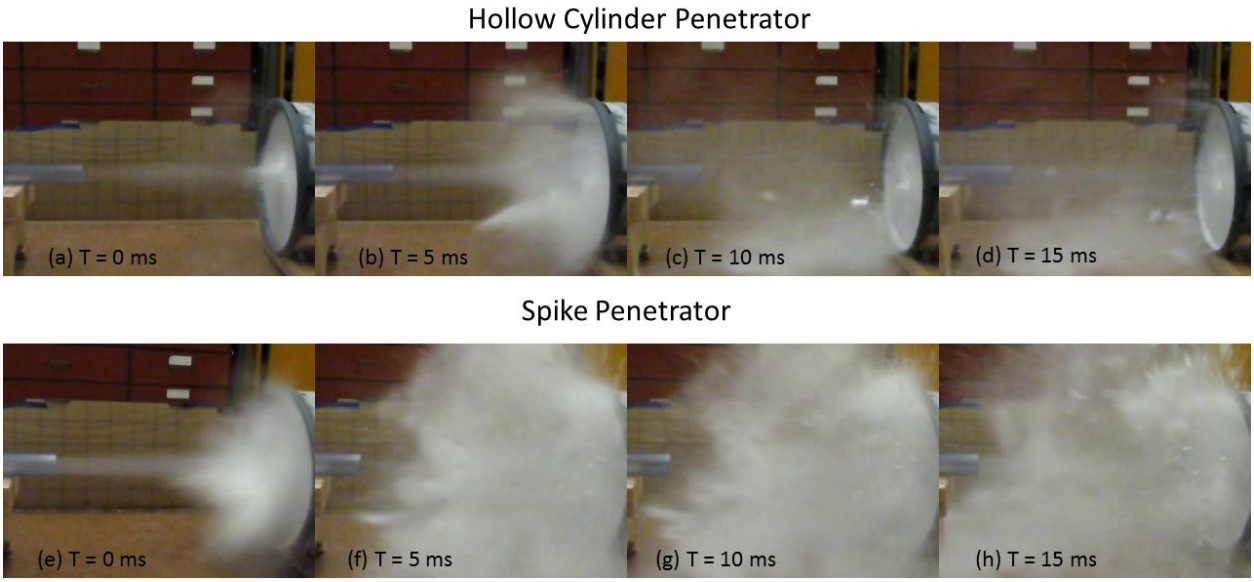

Figure 21: Ejecta Patterns for Low Pressure Impacts

High Pressure Gas Gun

The results from the air gun and ANSYS needed to be scaled up to higher velocity shots of interest to the hard landing concept being investigated. This was done using the RAM Accelerator in gun mode.

Wood Targets

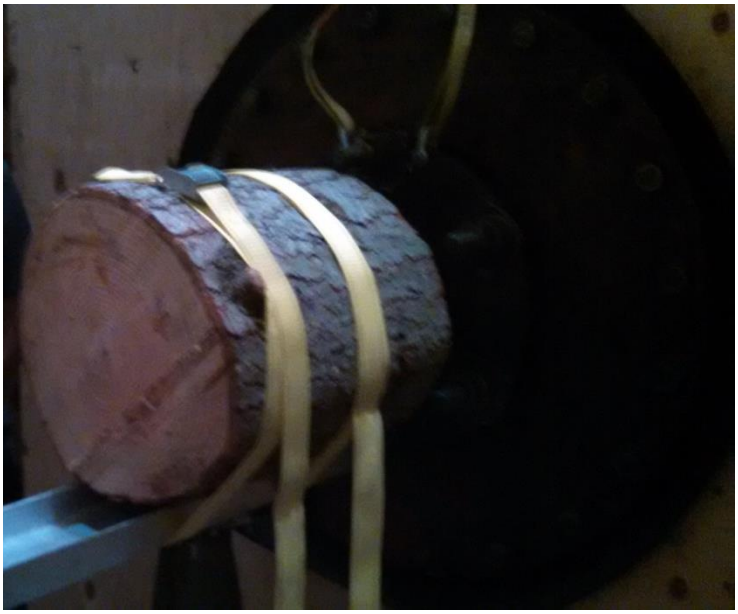

Figure 22: Wood Target for RAM Test Shots

In order to test the RAM system, wood logs 36cm in diameter and 62 cm in length were used as targets due to ease of use. It was only expected to verify operation of the gun system. The high speed footage provided good insight into the behavior of volatiles in the ejecta.

As the cylindrical projectile impacts the wood, a vapor plume appears which is most dense back along the original path of travel. There was only a small separation between the projectile and the obturator, but there is still visible interaction between both the obturator and the wave of gas pushing it and the plume sent back by the initial impact.

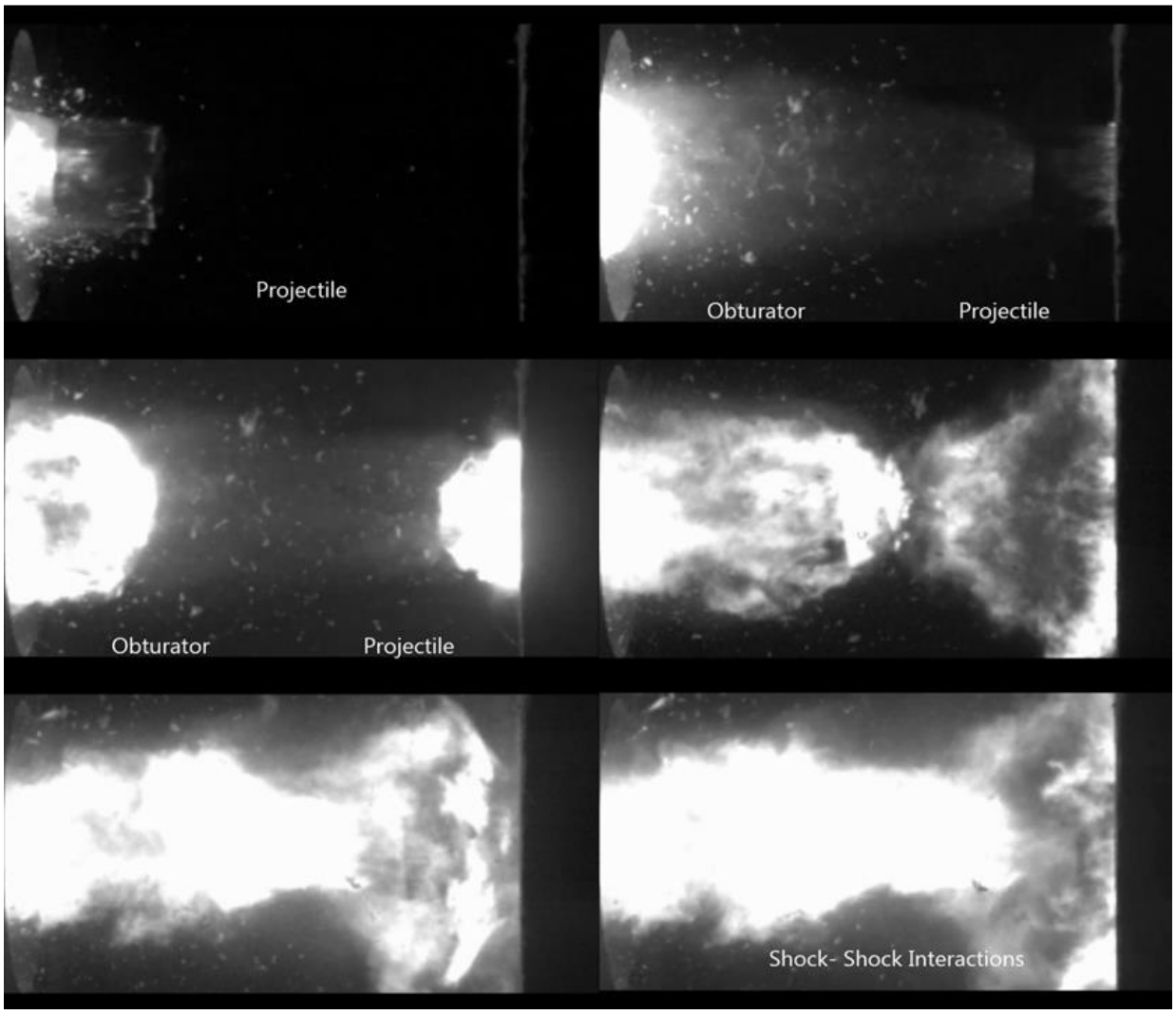

Figure 23: High Speed Shots of 1.4 km/s Shot into Wood Target with Cylinder and Obturator

The wood target mostly maintained its original shape and dimension. This affected the intuition of how a larger ice target would behave under similar conditions. Wood is a fibrous material which prevented large amounts of fracturing through the material. This only became apparent after ice impacts and the explosive fracturing behavior.

Figure 24: Wood Target After High Velocity Impact

30 gallon targets

For high velocity shots, the ice targets fracture almost completely. The 30 gallon containers were destroyed. Ice has no fibers to absorb the energy of an impact, thus the energy is propagated through the material easily and quickly. The difference between the wave propagation pattern from different projectile shapes is visible when observing the damage to the cans.

For the conical projectile, the pressure wave travels down and through the entire can in the direction of the original shot. The pattern is similar to the shock patterns produced by a supersonic nose cone.

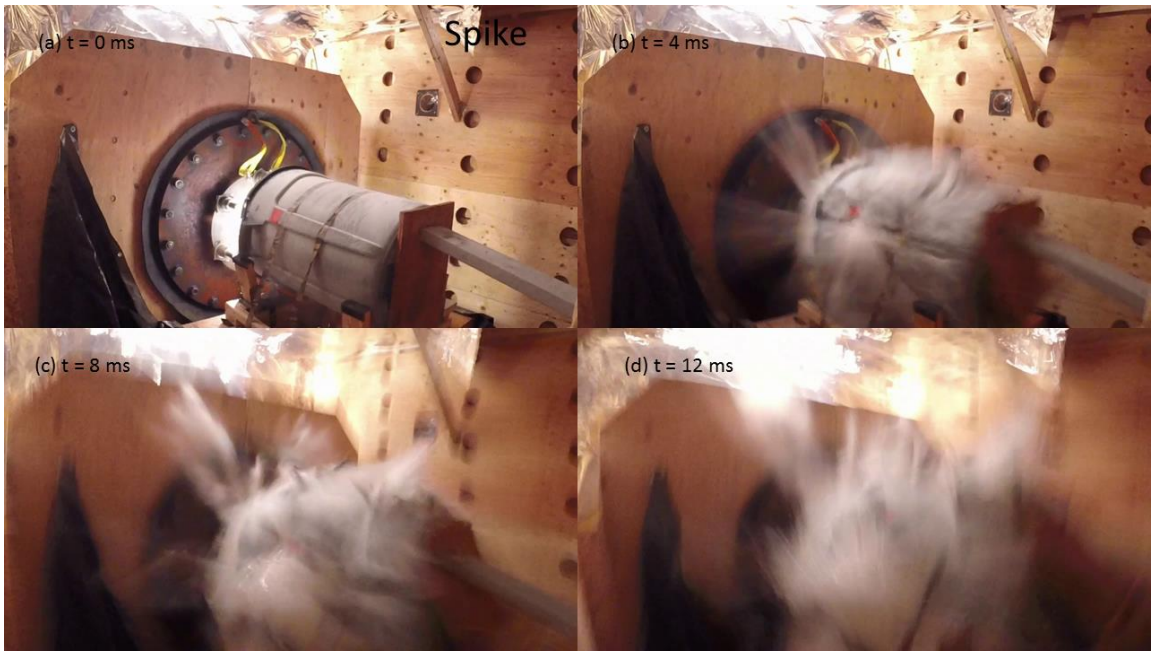

Figure 25: 30 Gallon Ice Target Behavior During Conical (Spike) Projectile Impact

For the hollow cylindrical projectile impacts, the damage does not travel down through the can with the same intensity. A greater amount of energy is reflected back sending more material back along the original path of the impact.

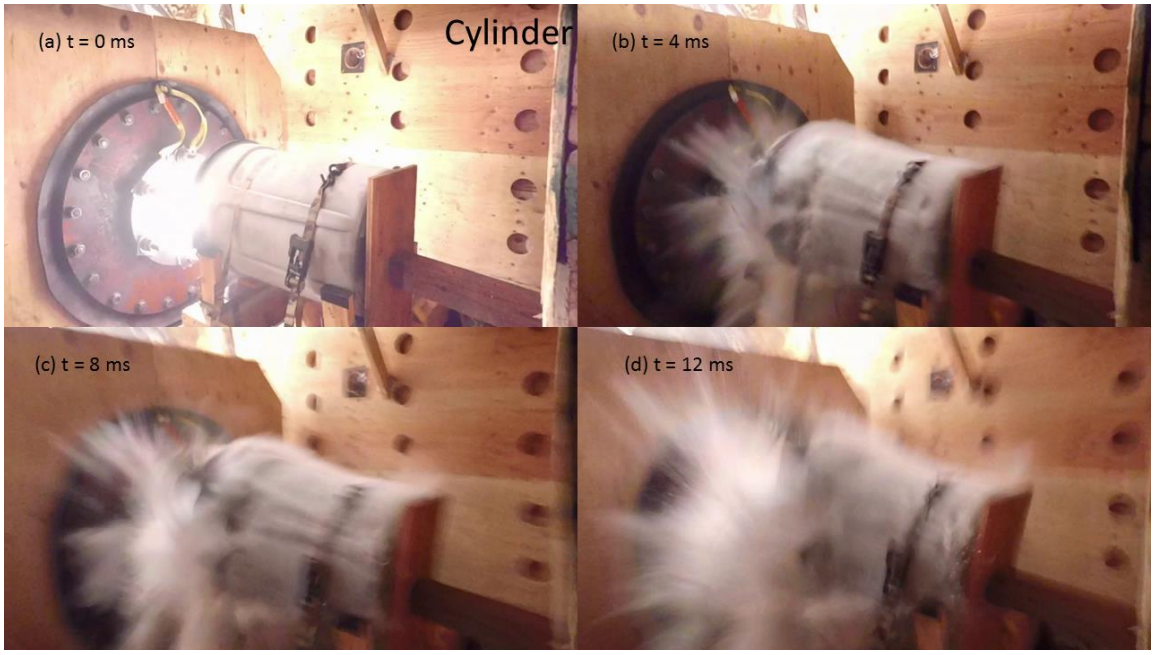

Figure 26: 30 Gallon Ice Target Behavior During Cylindrical Projectile Impact

High speed images observed similar results to the air gun in plume shape. The cylindrical projectile allows air to pass through it which causes a greater separation back to the obturator.

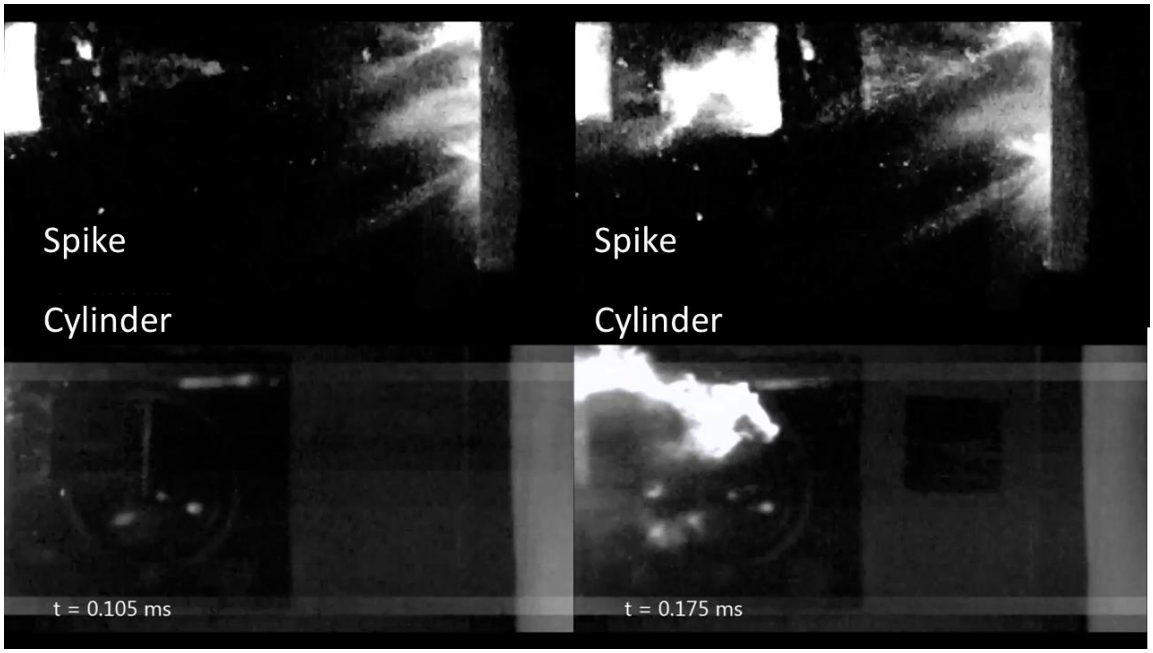

Figure 27: Conical (Spike) and Cylindrical Projectiles Pre-Impact

The conical projectile produces a hollow cone of ejecta, which the obturator is largely unaffected by. The cylindrical projectile produces a collimated ejecta field which the obturator travels directly through.

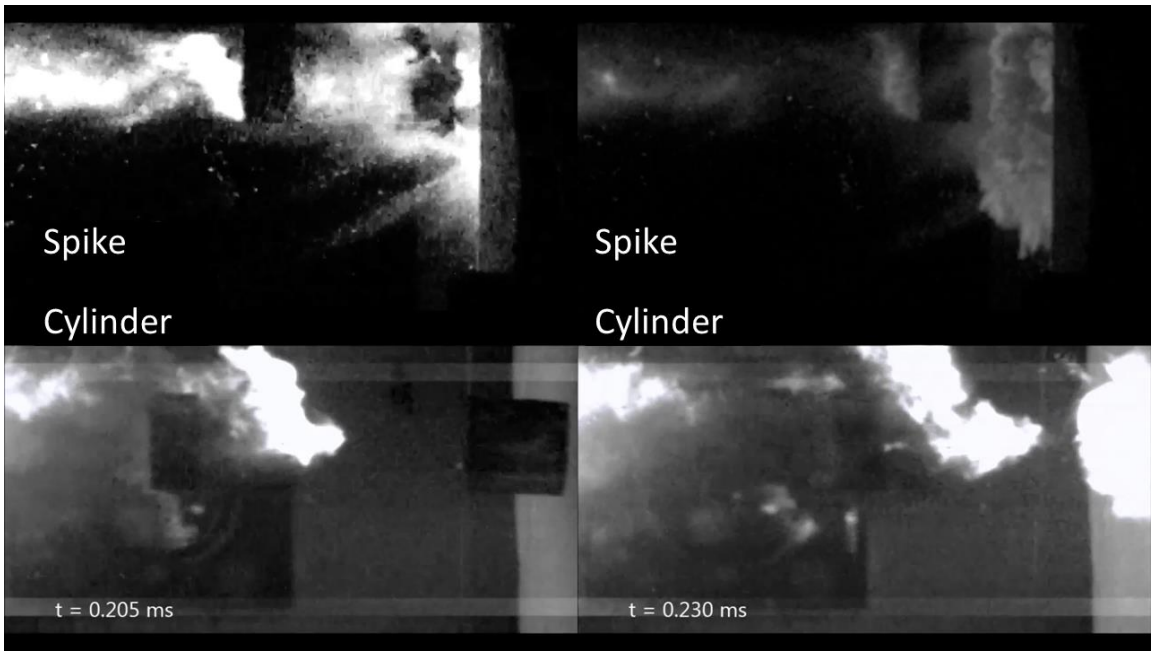

Figure 28: Initial Impact of Conical and Cylindrical Projectiles

The obturator in the conical impact travels with little to no effect from the ejecta plume. The obturator from the cylindrical impact travels directly through the plume resulting in visible alteration of the ejecta field.

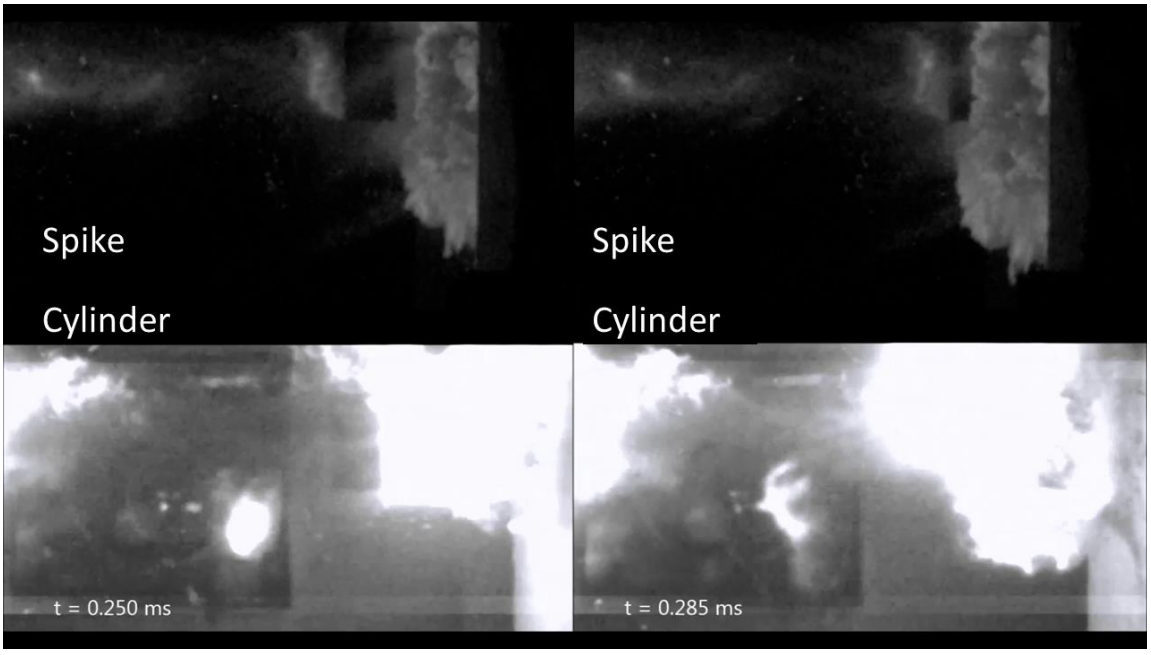

Figure 29: Obturator Interaction with Conical and Cylindrical Ejecta Plumes

96 gallon targets

Due to the total can destruction of the 30 gallon shots, penetration depth was not measured. Also, the boundary conditions of the targets may have affected the target behavior due to reflecting energy back through the target. These unclear boundary conditions are one of the main reasons for increasing the ice target size to 96 gallons. Also, one of the 96 gallon cans was filled only with ice and one was lined with foam insulation.

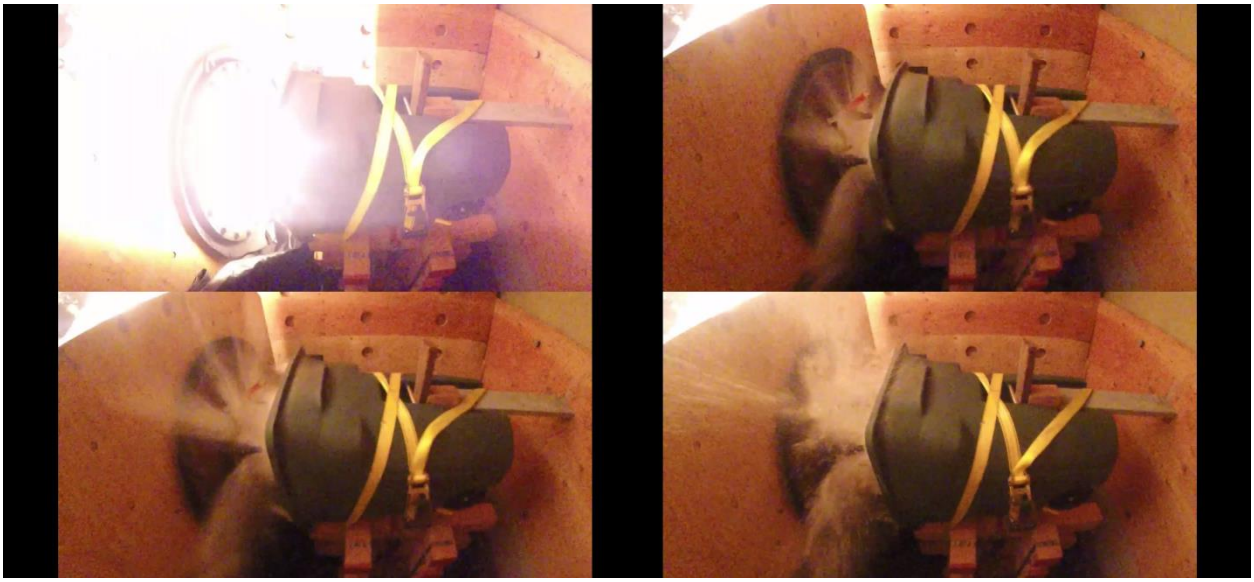

Figure 30: 96 Gallon Can Without Insulation

The large uninsulated can had less damage to the can during its impact. There was still interaction with the can which is demonstrated by elastic deformation along the walls of the can. Different colored layers in the ice allowed for an estimation of penetration depth $d{\sim}33\ cm$.

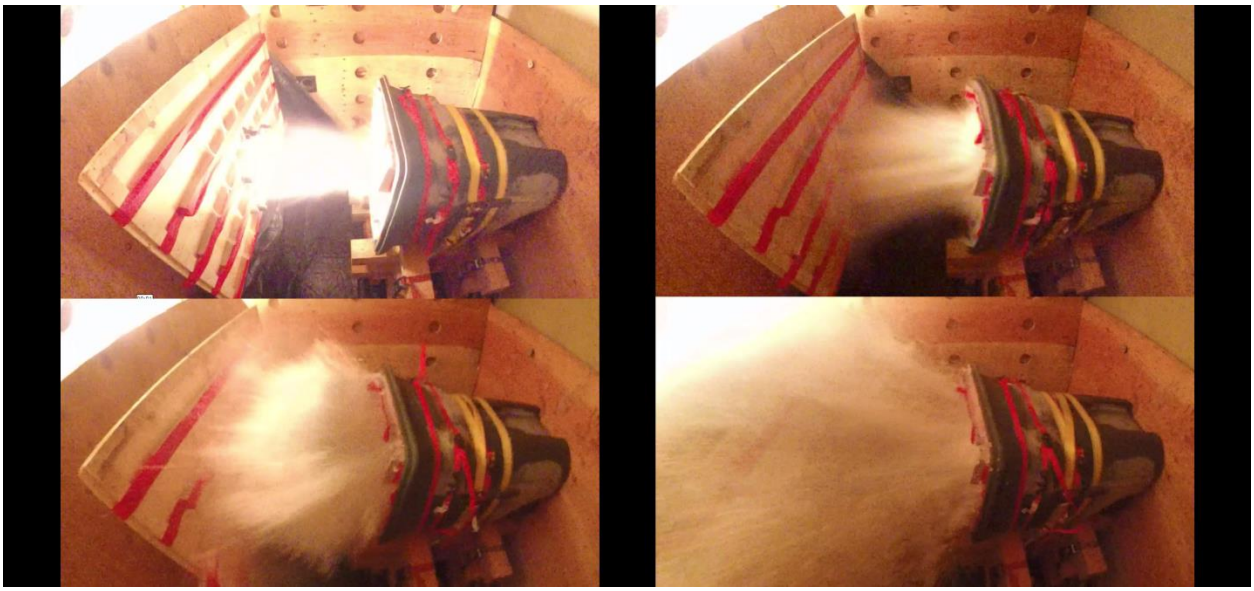

Figure 31: 96 Gallon Can With Insulation and Splash Catch Board

For the insulated can impact, the damage to the can was lowered even further than the non-insulated can, but the can still had elastic deformation during impact. A splash catch board was set up to try and measure the density gradient of the ejecta plume. The energy of the impact of ejecta with the splash board was too great for containers attached to the board. There was centralized damage on the board which confirms some collimation of the debris.

Figure 32 shows the cylindrical projectile debris removed from the 30 gallon target and the insulated 96 gallon target. Both impacts were at $\sim 1.2 \frac{km}{s}$, but the damage to the projectile is much greater for the smaller target. The difference in projectile fracturing suggests that boundary conditions have a significant effect on impact characteristics, but more data are necessary for affirmation.

Figure 32: Cylindrical Projectile Debris for 30 Gallon and 96 Gallon Insulated Targets

Figure 33 is a conical projectile after impact in a 30 gallon ice target. The projectile maintained most of its original shape, which demonstrates higher structural integrity than the cylindrical projectile under similar impact conditions. This shape can be useful in payload protection during impact.

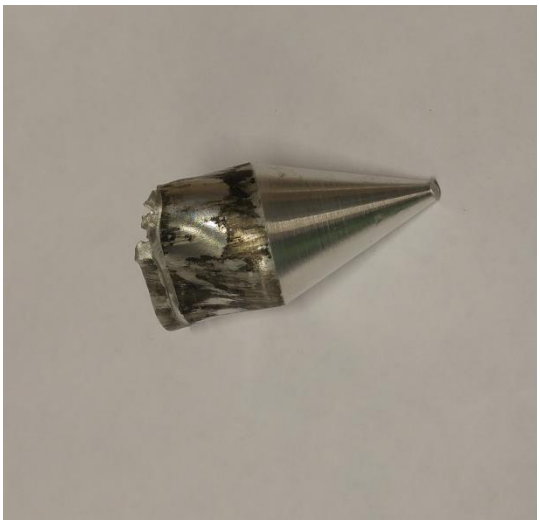

Figure 33: High Pressure Gas Gun Conical Projectile Debris

Discussion

The proposed hard landing system of two projectiles, a hollow cylindrical pre-impactor followed by a payload projectile with aero-braking surfaces, can be designed to use ejecta and plume characteristics of a cylindrical impact to reduce the speed of an instrument payload to within survivable impact velocities. The cylinder shape leads to more concentrated target fracturing and directed ejecta stream. The conical shape provides structural integrity and payload protection. Further analysis is necessary for measuring the density gradient of the plume. Separation of the first and second projectile will need to be deliberate during a landing of this system. The required separation distance will be an apparent result of a computationally consistent model of the plume.

Next Steps

The next few steps are already in progress. The Pykrete lined 96 gallon cans have temperature sensors installed at 7”, 14”, and 21” penetration depths. The measured change of temperature will be an indicator of possible phase change during impact. These cans will also provide additional data points for the boundary condition effects on impacts.

Splash Plate

During the shots with the Pykrete 96 gallon cans, a large Mylar splash plate will be used instead of the splash board to measure plume density collimation. A conical and cylindrical projectile will be used for comparison.

Flour Drop

Lower energy plume visualization can be achieved by dropping projectiles into a flour target. This will be a quick and easily repeatable method for comparing multiple projectile shapes.

Multi-Projectile High Pressure System

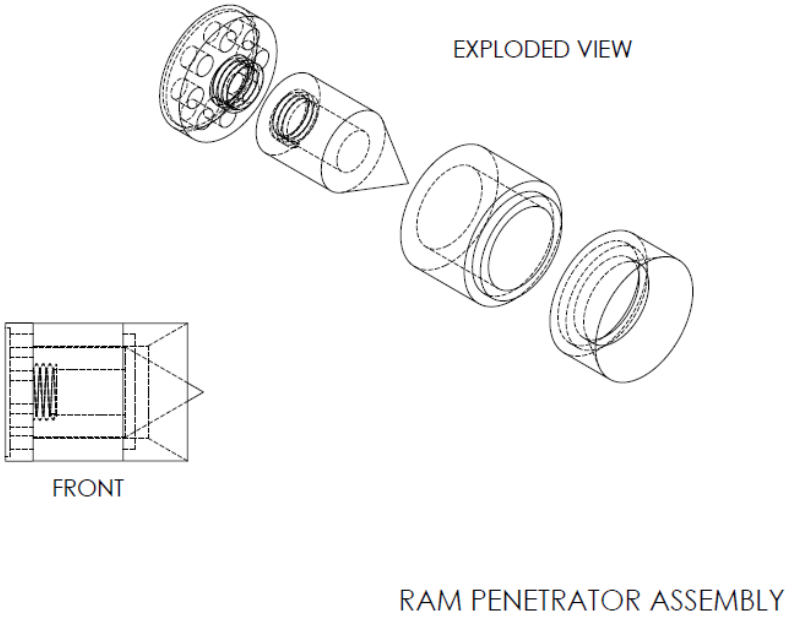

Figure 34: Multi-Projectile for RAM

A multiple-projectile design has been made for use in the helium gas gun. The first projectile is an aluminum and steel composite cylinder with a straight bore. The second projectile is a Lexan and aluminum composite cone with a circular fin for aero-braking. There is a section in the second projectile that could house either a small electronic component or circuit. This payload may not be able to survive the acceleration of the initial shot so it may not be included in the final experiment. The main instrumentation for this shot would be the magnetometers for velocity measurements and high speed imagery for plume interaction.

Accelerometer Circuit Shots

For the air gun, the two projectile system shown in figure 14 will house an accelerometer circuit. The conical projectile will be shot by itself and then shot in conjunction with a cylinder. The acceleration data from these shots can be compared. The composite shot requires a deliberate separation to ensure proper plume interaction.

Helicopter Drop

A system is currently being designed for a drop from a helicopter onto a glacier. The second projectile for this system will use aerodynamic surfaces for separation and then interaction with the plume.

CFD Modeling

The interior surface of the cylindrical projectile acts as a nozzle for the fractured target material. CFD modeling of a composite fluid can analyze various shapes internal to the cylinder to maximize the ejecta speed and plume density variation.

Dynamic Modeling

Dynamic modeling systems such as LS-Dyna can be used to create a complex model for impact phenomena and plume characteristics.

References

[1] R. Winglee and C. Truitt, "Sample Return Systems For Extreme Environments," 2012.

[2] I. Grey, M. Burchell and N. Shrine, "Laboratory Investigations of the Temperature Dependence of Hypervelocity Impact Cratering in Ice," *Adv. Space Res.,* vol. 28, no. 10, pp. 1527-1532, 2001.

[3] National Research Council, "Committee on the Effects of Nuclear Earth-Penetrator and Other Weapons, Effects of Nuclear Earth Penetrator and Other Weapons," National Research Council, 2005.

[4] J. Li, Z. Wei and C. Wu, "Preparation and properties of novel building materials," *Elsevier Materials,* vol. 67, pp. 464-468, 2014.

Appendix

Matlab code for radius requirement for plume estimation

```
clear all
close all
clc

a=10^5;
mp=5;
ri=0.05;
v=4000;
cd=0.5;
h=80;
r=ri:0.01:0.5;

A=pi.*r.^2;
F=mp*a;
rhoi=2*F./(v^2*cd.*A);

rho=rhoi.*(h./r).^2;

plot(r,rho)
xlabel('r (m)- radius of impactor')
ylabel('\rho (kg/m^3) density at impact site')
```